

Microstructure and properties of ZrO_2 - $ZrSiO_4$ ceramic composites obtained by reactive sintering

E. G. D. Santanna¹, P. L. Gomes¹, J. E. V. Amarante², M. F. R. P. Alves³, R. O. Magnago⁴, C. dos Santos^{1,4*}

¹Universidade Federal Fluminense, Escola de Engenharia Industrial Metalúrgica de Volta Redonda, 27276-210, Volta Redonda, RJ, Brazil

²Universidade Federal Fluminense, Faculdade de Odontologia, Instituto de Saúde de Nova Friburgo, 28625-650, Nova Friburgo, RJ, Brazil

³Universidade de Aveiro, 3810-193, Aveiro, Portugal

⁴Universidade do Estado do Rio de Janeiro, Faculdade de Tecnologia, 27537-000, Resende, RJ, Brazil

Abstract

ZrO_2 - $ZrSiO_4$ composites obtained from mixtures of 3Y-TZP and SiO_2 powders were investigated. Commercial 3Y-TZP powder and mixtures containing 5 or 10 wt% of SiO_2 were prepared. Specimens ($n=10$ /group) were uniaxially compacted and sintered at 1500 °C-2 h (5 °C/min). Sintered samples were characterized by their relative density, X-ray diffraction, scanning electron microscopy, energy dispersive spectroscopy, and Vickers nanoindentation. The monolithic- ZrO_2 sample presented full densification while increasing of SiO_2 content progressively reduced the relative density. The crystalline phases presented in composites were tetragonal- ZrO_2 , cubic- ZrO_2 , $ZrSiO_4$, monoclinic- ZrO_2 , and residual cristobalite (SiO_2). Microstructural analysis indicated a distribution of zirconia grains, with heterogeneous regions rich in SiO_2 surrounded by $ZrSiO_4$ grains. Vickers hardness of 1590±19 HV for monolithic ZrO_2 , 1475±27 HV for ZrO_2 -5 wt% SiO_2 , and 1336±32 HV for ZrO_2 -10 wt% SiO_2 were obtained indicating reduction in hardness with increasing SiO_2 fraction. Furthermore, a reduction in fracture toughness was observed (7.2±0.8, 6.7±0.5, and 5.4±1.0 MPa.m^{1/2}, respectively) and Young's moduli measured were 174.1, 169.7, and 225.9 GPa, respectively. These experiments demonstrated, preliminarily, that the ZrO_2 - $ZrSiO_4$ composite, based on 3Y-TZP- SiO_2 powder mixtures, can achieve good levels of densification and present reasonable mechanical properties, requiring improvements in microstructural homogenization. However, the presence of SiO_2 and $ZrSiO_4$ can improve the adhesion of zirconia to resin cement, requiring future studies focused on adhesion to confirm its viability.

Keywords: ceramic composites, ZrO_2 - SiO_2 system, reactive sintering, phase transformations, mechanical properties.

INTRODUCTION

Yttria-stabilized zirconia (ZrO_2 - Y_2O_3) presents potential for applications in the dental market due to its mechanical properties, biocompatibility, and aesthetics similar to the teeth [1-3]. The predominance of the tetragonal zirconia crystalline phase is a potential factor of its mechanical strength, which can be obtained by stabilization with 3 mol% Y_2O_3 . In this microstructural condition, when the ceramic is subjected to mechanical stress, a phenomenon of phase transformation from tetragonal- ZrO_2 to monoclinic- ZrO_2 (t→m) occurs, resulting in a localized increase in the volume of zirconia grains (the order of 3-5%), hindering the crack propagation, and improving fracture toughness [4-6]. ZrO_2 -3 mol% Y_2O_3 ceramics (3Y-TZP) usually present hardness around 1250 HV, Young's modulus between 190 and 210 GPa, flexural strength greater than 800 MPa, and fracture toughness between 6 and 9 MPa.m^{1/2} [7]. These mechanical properties, along with chemical stability and biocompatibility, make 3Y-TZP ceramics a very interesting option for the manufacture of dental prostheses and/or

components of implant systems [8-10]. However, the use of 3Y-TZP for dental applications has some specific problems, such as hydrothermal degradation, also called aging, which Y-TZP ceramics can demonstrate when subjected to humid environments for prolonged periods and with cyclic loads, even at low temperatures, resulting in loss of long-term mechanical properties [11, 12]. Degradation media such as distilled water, artificial saliva, and an acidic solution of pH 2.5 can influence the surface of zirconia, leading to the rupture of Zr-O-Zr bonds and the formation of Zr-OH or Y-OH bonds, creating surface stress, accelerating the martensitic transformation which tetragonal crystals transform into monoclinic (t→m). Degradation can propagate from the surface to the interior of the zirconia through the grain boundary. Usually, the t→m transformation of a zirconia grain increases its volume, which should compress the crack, preventing its propagation; however, with the penetration of moisture, the crack would propagate to more internal layers, releasing surface grains, resulting in increased surface roughness, compromised mechanical properties of the material and increased risk of critical failures [13-15].

Y-TZP ceramics have low adhesion with resin cements, compared to porcelains and lithium disilicate glass-ceramics, mainly due to their high crystallinity and low amount of amorphous glassy phase, responsible for the chemical bond

*claudineisvr@gmail.com

<https://orcid.org/0000-0002-9398-0639>

between the dental ceramic and the resin, being a disadvantage to its use in dental restorations [16, 17]. Traditional cements such as zinc phosphate or modified ionomers guarantee adequate clinical adhesion of zirconia restorations, however, the use of adhesive cementation is more recommended as it ensures greater retention and marginal adaptation, which leads to greater resistance to fracture and better aesthetics. To obtain reliable adhesion on ceramic surfaces, treatments based on physical retention through blasting and ceramic/substrate chemical bonding through silicates, silanes, and/or primers are required [18]. Blasting with aluminum oxide (Al_2O_3), followed by silicization of zirconia with subsequent silanization is suggested as a surface treatment of Y-TZP ceramics, pre-adhesive cementation [19, 20]. In this tribo-chemical technique, the surface of the zirconia is blasted with aluminum oxide particles and Al_2O_3 particles modified with silica (SiO_2), in which the pressure of the blasting leads to an incrustation of the silica of the particle on the ceramic surface, making it rougher and chemically reactive to silane, therefore, more adherent. A thin silica layer of approximately 15 μm can be obtained on this ceramic substrate [21, 22]. Tests evaluating the immediate adhesive forces and after 6 months of storage in the water of resin cements on the adhesion of pre-treated zirconia under various conditions indicated that cements containing the monomer MDP (methacryloyloxydecyl dihydrogen phosphate) could cement the ceramic. In the evaluation of the 6-month period, it was observed that the resistance of the group of samples treated with silica did not vary significantly, while the group without this treatment and with sandblasting had a marked decrease in its properties [23].

Zirconium silicate, or zircon (ZrSiO_4), is a ceramic material with a low coefficient of thermal expansion of $4 \times 10^{-6} \text{ }^\circ\text{C}^{-1}$ [24] that has a wide range of refractory or nuclear applications due to its chemical stability in fluid or vitreous media. However, its flexural strength and fracture toughness are limited for structural applications and are of the order of 200-300 MPa and 2-3 $\text{MPa}\cdot\text{m}^{1/2}$, respectively [25]. This oxide doesn't undergo significant chemical changes up to around 1680 $^\circ\text{C}$, the temperature at which it dissociates into SiO_2 and ZrO_2 , and the temperature at which dissociation begins may be reduced due to the increase in the impurity content in the material [26, 27]. Another characteristic of this material is its low sinterability; sintering of ZrSiO_4 starting from synthesized powders is difficult and, sometimes, maximum densification is not achieved, only be achieved with the use of special sintering techniques and spark plasma sintering (SPS) [28-30].

An alternative to reduce the resistance to hydrothermal degradation characteristic of 3Y-TZP ceramics is introducing a second phase as reinforcement or even increasing the cubic ZrO_2 proportion at the expense of tetragonal zirconia [31, 32]. Furthermore, in order to contribute to the improvement of adhesion between the zirconia-based material and resin cement, a strategy to be developed can be the creation of a Y-TZP/ ZrSiO_4 composite [33]. This work aimed to develop a composite from mixtures of 3Y-TZP and SiO_2 powders in

different proportions, aiming to identify the most important microstructural and crystallographic aspects to combine phase transformations and densification promoted during sintering.

EXPERIMENTAL

The ceramic materials used in this work were commercial powders of zirconia (TZ-Yellow-SB-E, Tosoh) and silica (83340 Quartz, Fluka). Tables I to III present the main characteristics of the raw materials. The zirconia powder was submitted to calcination thermal treatment at 800 $^\circ\text{C}$ for 60 min, using a furnace with MoSi_2 resistance (ME-1800, Fortelab) aiming to eliminate organic compounds.

A monolithic sample of 3Y-TZP and mixtures containing 3Y-TZP with SiO_2 contents of 5 or 10 wt% were prepared. For powder mixtures, ethyl alcohol was used. The suspension was mixed using a mechanical shaker (NT 137) for 60 min at 150 rpm. Subsequently, the mixtures were placed in an oven at 100 $^\circ\text{C}$ for 24 h for drying. Then, the powder mixtures were deagglomerated using a mortar and pestle and sieved with a 63 μm sieve. 4% of PVA (polyvinyl alcohol) binder was added to the mixtures, and then the material was returned to the mortar for complete homogenization and then sieved again. Specimens ($n=10/\text{group}$) were uniaxially compacted at 80 MPa for 45 s and sintered at 1500 $^\circ\text{C}$ for 2 h, using a furnace (ME-1800, Fortelab) with heating and cooling rates of 5 $^\circ\text{C}/\text{min}$.

The starting powders were characterized by X-ray diffraction (XRD) and scanning electron microscopy (SEM). The apparent density of the sintered samples was determined by Archimedes' principle, using a precision scale (0.001 g) (Discovery, Ohaus), and the relative density calculations were determined, correlating the apparent density with the theoretical density obtained using the rule of mixtures, considering in the calculations the proportions of each phase in the sintered samples and adopting $\rho_{\text{ZrO}_2}=6.05 \text{ g}/\text{cm}^3$, $\rho_{\text{SiO}_2(\text{quartz})}=2.65 \text{ g}/\text{cm}^3$, $\rho_{\text{SiO}_2(\text{cristobalite})}=2.32 \text{ g}/\text{cm}^3$, and $\rho_{\text{ZrSiO}_4}=4.60 \text{ g}/\text{cm}^3$, according to ASTM C20-17 [34-38]. The phases present in the sintered samples were identified by XRD, using a diffractometer (X'Pert Pro, Panalytical) with $\text{CuK}\alpha$ radiation ($\lambda=1.54 \text{ \AA}$) in the 2θ range between 10 $^\circ$ to 90 $^\circ$, an angular step width of 0.05 $^\circ$ at a time of 2 to 3 s/step. Furthermore, sintered samples were analyzed using a scanning electron microscope (SEM/FEG, 7100FT, Jeol) with an energy dispersive spectroscope (EDS, X-Max, Oxford) with an 80 mm^2 detector. For microstructural evaluation, the polished surfaces of the sintered samples were thermally etched at 1390 $^\circ\text{C}$ for 15 min, with a heating rate of 25 $^\circ\text{C}/\text{min}$, and a thin layer of gold was deposited using a metallizer (K550X, Quorum Technol., UK), with 30 mA of current for 2 min. The evaluation of the grain size distribution of the sintered samples was made using the Image J software for the images obtained by SEM.

Young's modulus and nanohardness of the samples were obtained using an instrumented ultra-microhardness tester (DUH 211S, Shimadzu, Japan) with a 115 $^\circ$ triangular

Table I - Chemical composition (wt%) of the starting $ZrO_2(Y_2O_3)$ (TZ-Yellow-SB-E, Tosoh) powder (manufacturing data).

Y_2O_3	HfO ₂	Al ₂ O ₃	SiO ₂	Fe ₂ O ₃	Na ₂ O	ZrO ₂
5.2±0.5	<5.0	0.1~0.4	≤0.2	0.1	≤0.4	Balance

Table II - Chemical composition (wt%) of the starting SiO₂ (83340 Quartz, Fluka) powder (manufacturing data).

Ca	Fe	Na	K	Others*	SiO ₂
≤0.02	≤0.02	≤0.01	≤0.05	≤0.005	Balance

* Cd, Co, Cu, Ni, Pb, Zn.

Table III - Physical characteristics of the starting powders (manufacturing data).

Characteristic	ZrO ₂ (Y ₂ O ₃)	SiO ₂
Particle size (µm)	0.09	63
Density (g/cm ³)	6.05	2.65

pyramidal indenter. The tests were performed in loading and unloading modes, with no holding time at the maximum load, an indentation depth range of up to 10 µm, and maximum load values of 250, 500, 1000, 1500, or 1960 mN. Five measurements of indentation per load were collected in order to estimate the average values of the indentation modulus (E_{it}) and the correspondence between indentation hardness and Vickers hardness (HV). The Young's modulus (E) was calculated using the Oliver and Pharr model by [39]:

$$E_{it} = \frac{1 - \nu_s^2}{S\sqrt{\pi}} \cdot \frac{1 - \nu_i^2}{2A_p E_i} \quad (A)$$

where $E=E_{it}$ is dynamic Vickers nanoindentation, S is the contact stiffness between the indenter and the sample, A_p is the contact area, ν_i and E_i are Poisson's ratio (0.07) and Young's modulus (1140 GPa), respectively, ν_s was not informed to the user and was available in the equipment software. The contact area with the indenter (A_p) was calculated by:

$$A_p = 24.5 \cdot h_c^2 \quad (B)$$

where h_c (µm) is the indentation depth linked to the surface delimited by the contact area of the indenter with the sample and can be calculated by:

$$h_c = h_{max} - 0.75(h_{max} - h_i) \quad (C)$$

where h_{max} is the maximum indentation depth (µm) and h_i is the intersection point of the tangent line to the unloading curve, from the maximum force with the horizontal axis linked to the indentation depth (µm). The Vickers nanohardness (HV)

was calculated by averaging the measurements per load in each sample, according to:

$$HV = 189.1 \frac{F_{max}}{L^2} \quad (D)$$

where F_{max} is the maximum force (mN) and L is the average height of the triangle formed by the indentations of the indenter in the sample, measured from one of its edges to the opposite vertex. The recommendation of a minimum distance between indentations and/or edges was respected, being greater than 3 times the diagonal of the nearest indentation; calculation and conversions occurred according to the instructions in the equipment manual [39-41]. The fracture toughness of the samples was measured by the Vickers indentation method, using a microhardness tester (HMV-2-digital, Shimadzu, Japan) and measuring the indentation crack sizes observed in an optical microscope (BX51M, Olympus, Japan) up to 24 h after the hardness test was performed. Eq. E valid for Palmqvist crack type (relationship between crack length, c, and indentation length, a, $c/a < 2.5$) was used to estimate fracture toughness (K_{IC} , MPa.m^{1/2}):

$$K_{IC} = 0.0752 \frac{F}{c^{1.5}} \quad (E)$$

where F is the applied force (N) and c is the average distance of half the length of the median cracks (m).

RESULTS AND DISCUSSION

Fig. 1 presents SEM micrographs of the as-received powders used as raw materials. Silica particles had irregular shapes and sizes and zirconia particles were agglomerated due to the presence of binders. Thus, the grinding/homogenization step of these raw materials, as well as the previous calcination of the zirconia particles, had the main function of allowing a good dispersion of the materials.

The results of the relative density measurements of the sintered samples indicated 99.2±0.3%, 96.1±0.2%, and 93.9±0.3% for ZrO₂-monolithic and the composites ZrO₂-5 wt% SiO₂ and ZrO₂-10 wt% SiO₂, respectively. These results indicated that the presence of silica in the initial powder mixtures, as well as the phase transformations resulting from chemical reactions that occurred during sintering, created obstacles to full densification. Fig. 2 presents the X-ray diffractograms of the sintered samples and Fig. 3 shows the respective phase quantification obtained by Rietveld refinement. The results indicated that the SiO₂ phase inserted in the material composition generated structural changes in relation to the control group, monolithic ZrO₂ (3Y-TZP). In this group, only 85% tetragonal-ZrO₂ and 15% cubic-ZrO₂ were present when the material was sintered at 1500 °C-2 h. The addition of 5 wt% SiO₂ allowed the formation of about 4% of ZrSiO₄ by the direct chemical reaction between SiO₂ and ZrO₂, with a consequent increase in the cubic-ZrO₂ phase content (about 18%) probably resulting from the migration

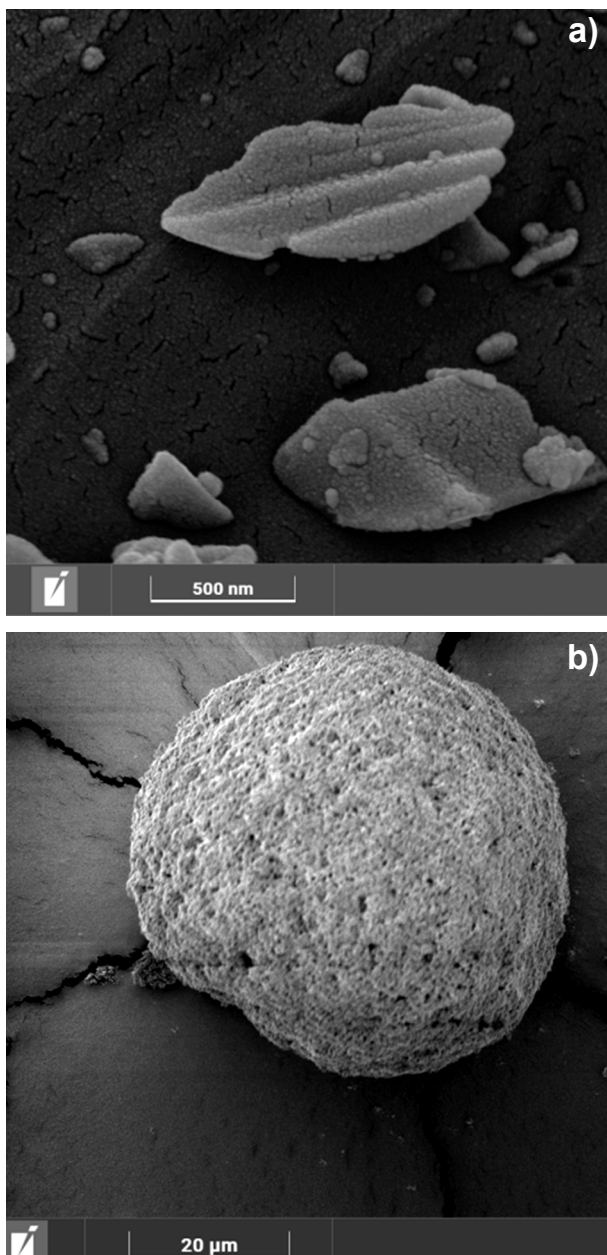


Figure 1: SEM micrographs showing the morphology of the SiO_2 (a) and ZrO_2 (b) powders.

of Y^{3+} ions for the cubic zirconia grains and the appearance of 3% monoclinic- ZrO_2 arising from the destabilization of tetragonal grains by the stoichiometric alteration resulting from the chemical reactions previously presented. The composites resulting from the addition of 10 wt% SiO_2 to zirconia had the same crystalline phases but with an increase in the amount of ZrSiO_4 (10.1%) and the presence of 1.2% cristobalite (unreacted SiO_2 with zirconia).

Figs. 4 to 6 show the micrographs of the compositions obtained by SEM. It was observed that the monolithic 3Y-TZP zirconia (Fig. 4) exhibits a bimodal grain size distribution, with a matrix of small grains (less than 1 μm) characteristic of the tetragonal phase with some slightly larger dispersed grains (between 1 and 2 μm) typical of the

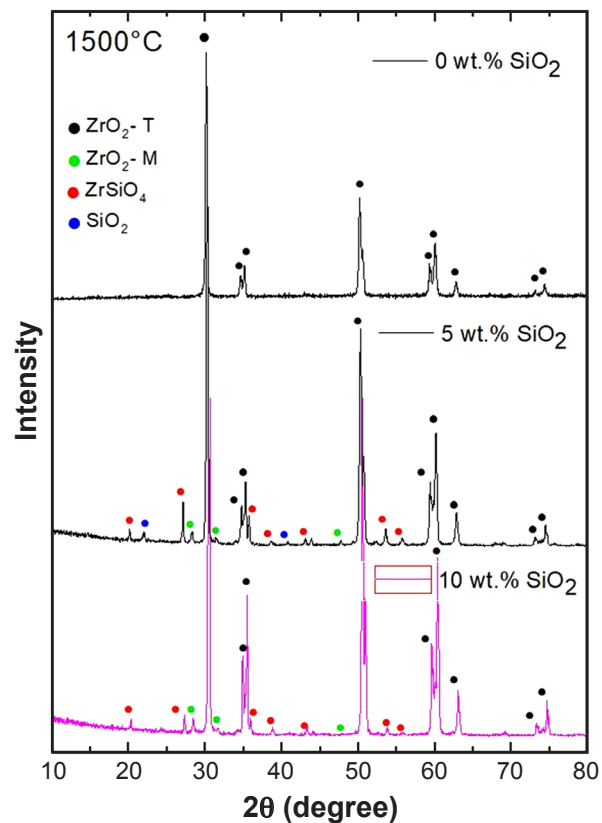


Figure 2: X-ray diffractograms of samples sintered at 1500 °C-2 h with 0, 5, and 10 wt% SiO_2 .

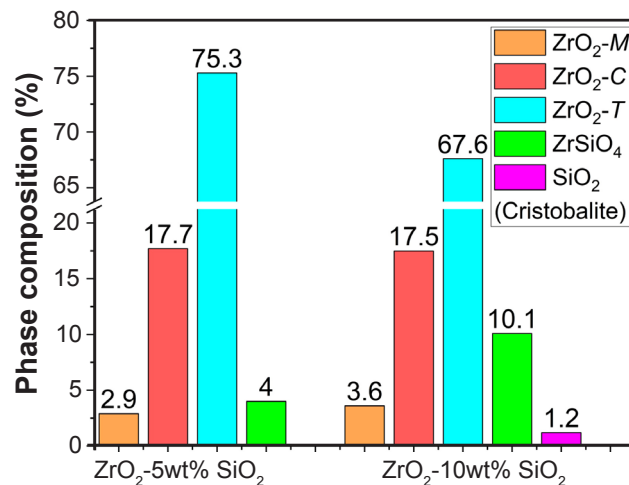


Figure 3: Phase quantification of composites sintered at 1500 °C-2 h for different compositions.

cubic phase [42]. In the composition with 5 wt% SiO_2 (Fig. 5) and 10 wt% SiO_2 (Fig. 6), SiO_2 (dark phase) was residual, non-reacted original SiO_2 particles, which were surrounded by a region rich in zircon (ZrSiO_4) with some small and tetragonal grains dispersed in its interior. This zircon region, in turn, had an interface of large grains of the cubic phase (around 3 to 5 μm) that performed its separation from the matrix composed of small grains of tetragonal zirconia. The lighter gray color in each image refers to the zirconia grains, whether cubic or tetragonal, while the darker gray

refers to SiO_2 and the intermediate gray between the two tones is equivalent to ZrSiO_4 . Substantial improvements in the microstructural homogenization of composites could be obtained by applying improvements in the processing of powder mixtures such as high-energy milling or the use of more homogeneous silica particles, which would avoid the formation of unreacted regions of SiO_2 and optimize the formation of the ZrSiO_4 phase.

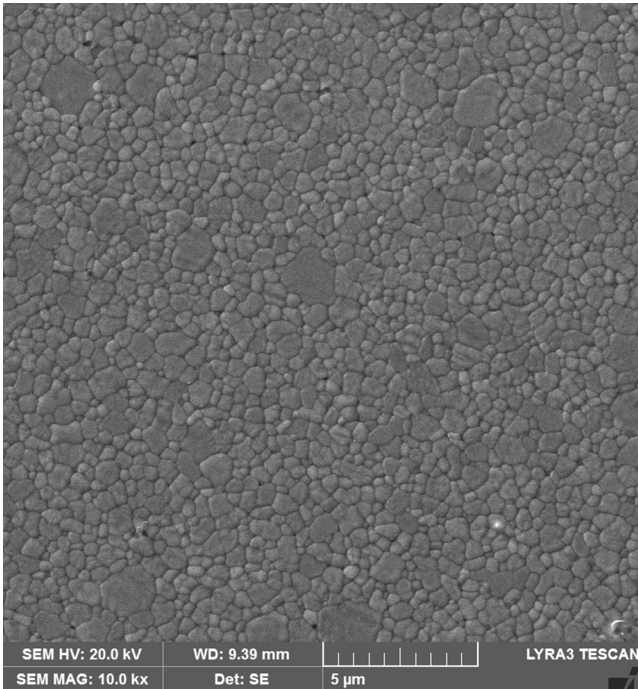


Figure 4: SEM micrograph of the monolithic 3Y-TZP sample sintered at 1500 °C-2 h.

Figs. 7 to 9 show the EDS mapping images for monolithic- ZrO_2 , ZrO_2 -5 wt% SiO_2 , and ZrO_2 -10 wt% SiO_2 composites, respectively. Furthermore, Fig. 10 presents EDS line scan profiles of the ZrO_2 -5 wt% SiO_2 composite. The monolithic zirconia sample (Fig. 7) exhibited a homogeneous distribution of its main elements (Zr, O, and Y) throughout the entire area analyzed. In the samples with 5 and 10 wt% SiO_2 (Figs. 8 and 9), this pattern was repeated over the regions of tetragonal zirconia grains; however, in the larger grains of cubic- ZrO_2 phase, a greater intensity of Y was observed; moreover, in the regions referring to ZrSiO_4 , the presence of an intermediate amount of all 3 main elements and a great intensity of Si was detected, although still less intense than the regions corresponding to SiO_2 where the highest intensity of Si was observed, together with O. Thus, the phases indicated in the X-ray diffraction patterns and microstructure results previously presented were confirmed. The phase quantification obtained by EDS and carried out in the analyzed region of the ZrO_2 sample doped with 10 wt% SiO_2 (Fig. 9) indicated 70.9% of ZrO_2 , 27.4% of ZrSiO_4 , and 0.9% of SiO_2 . The results of composition analysis by EDS line scan corroborated the statements about the composition of small and large grains of ZrO_2 , ZrSiO_4 , and SiO_2 formed.

Fig. 11a presents the Vickers hardness of the sintered samples, for different indentation loads. The monolithic 3Y-TZP samples sintered at 1500 °C-2 h showed uniform behavior regardless of load resulting in an average hardness of around 1590 HV. In the ZrO_2 -5 wt% SiO_2 sample group, an average value close to 1475 HV was obtained, and with an increase of SiO_2 to 10 wt% in the material composition, there was a reduction of almost 10% in hardness, with average values of 1355 HV. In general, the different applied

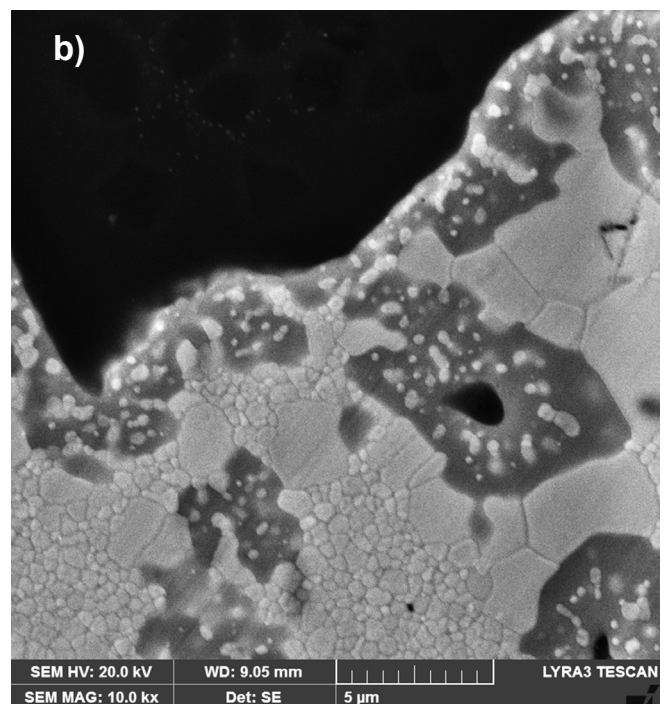
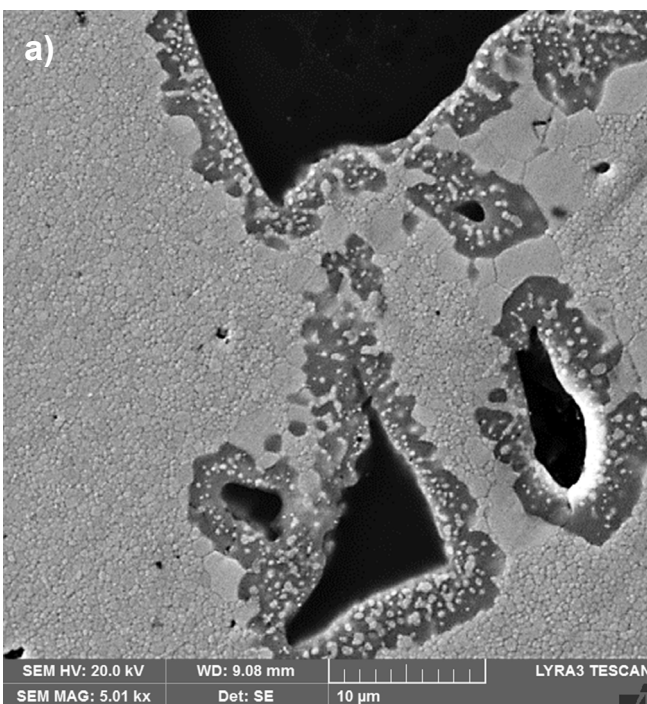


Figure 5: SEM micrographs of the sample ZrO_2 -5 wt% SiO_2 sintered at 1500 °C-2 h at different magnifications.

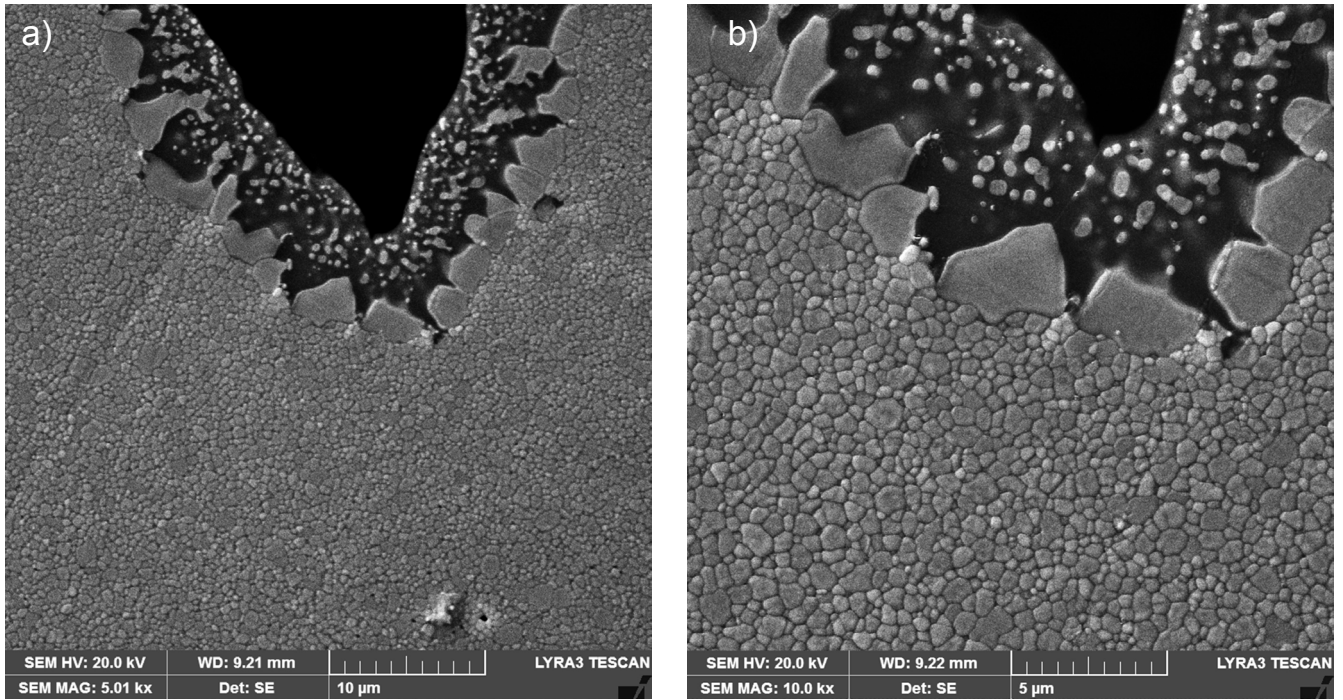


Figure 6: SEM micrographs of samples ZrO_2 -10 wt% SiO_2 sintered at 1500 °C-2 h at different magnifications.

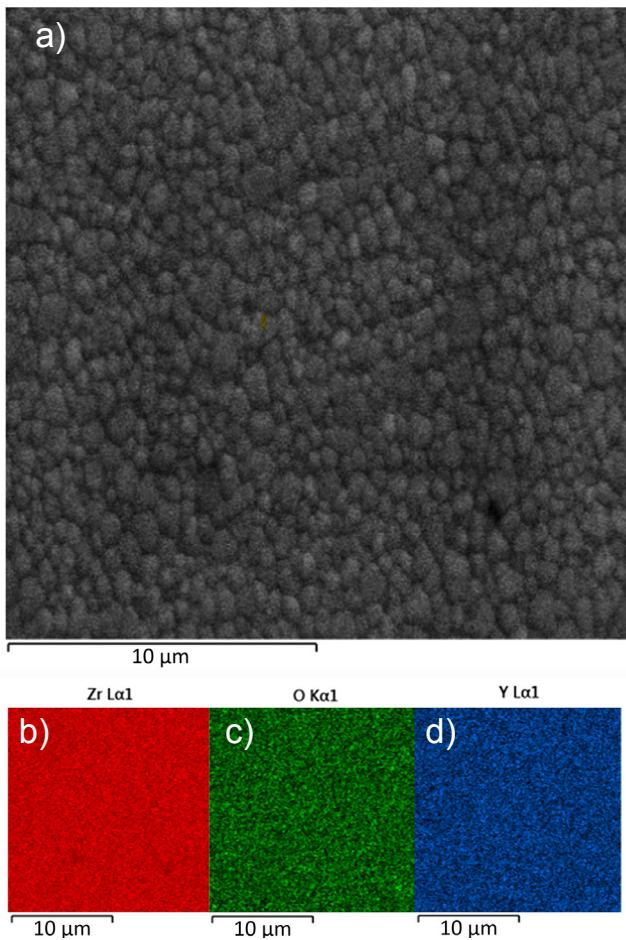


Figure 7: SEM micrograph (a) and corresponding elemental mapping images obtained by EDS for Zr (b), O (c), and Y (d) of the monolithic 3Y-TZP sample.

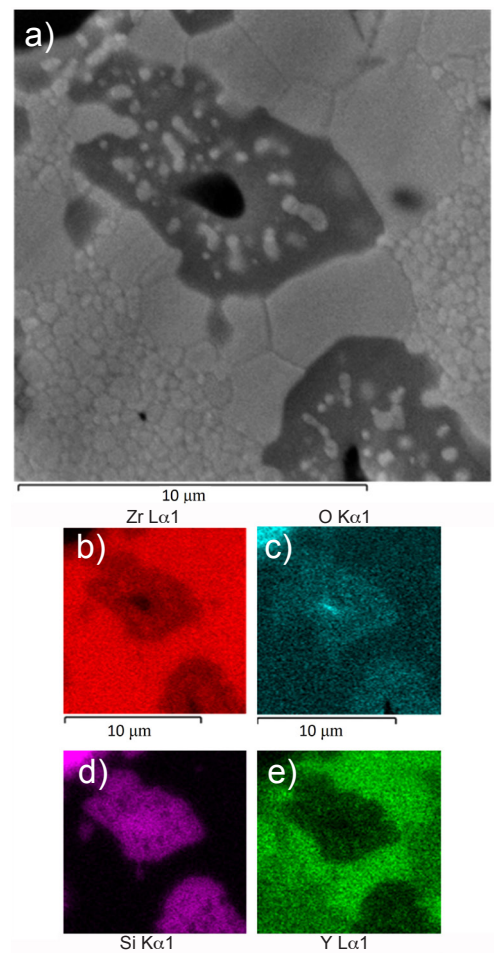


Figure 8: SEM micrograph (a) and corresponding elemental mapping images obtained by EDS for Zr (b), O (c), Si (d), and Y (e) of the sample with 5 wt% SiO_2 sintered at 1500 °C-2 h.

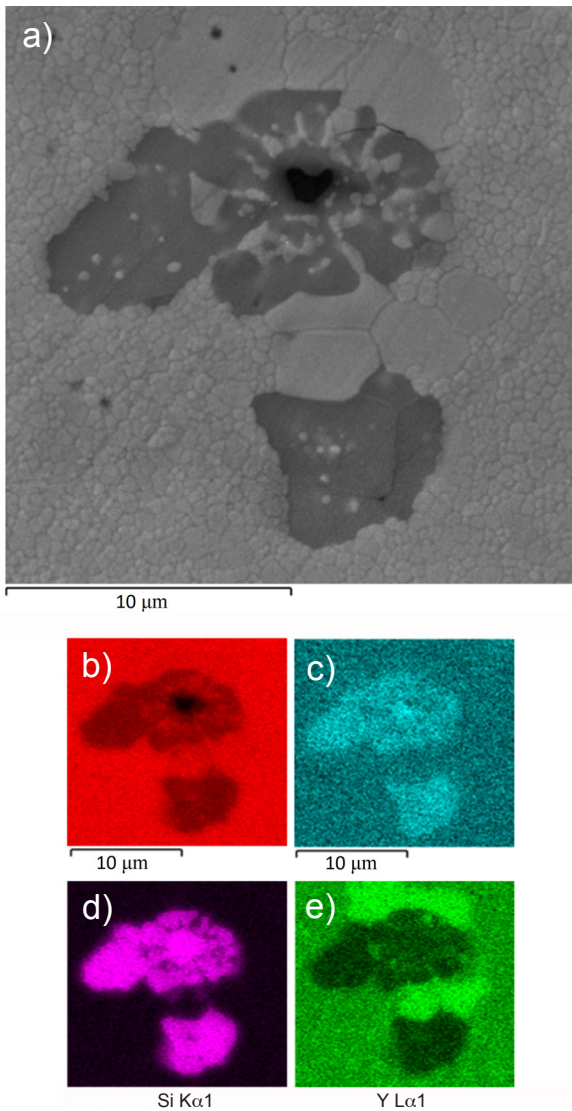


Figure 9: SEM micrograph (a) and corresponding elemental mapping images obtained by EDS for Zr (b), O (c), Si (d), and Y (e) of the sample with 10 wt% SiO₂ sintered at 1500 °C-2 h.

indentation loads did not indicate a well-defined trend profile for the mechanical behavior of the different materials. The measurement technique by nanoindentations has an elastic behavior different from traditional microhardness techniques, where the hardness values for 3Y-TZP ceramics are lower, around 1200 to 1300 HV [3, 13, 42, 43]. As in this type of technique with small loads, the indentations are in very small regions that can contain small or large grains, even regions of interaction with silica, since it was of interest to characterize the general behavior and not of a specific type of grain. The effect of the porosity of the material and the response to plastic strains around the indentation on the results are reduced, with this the hardness values are higher. From these impressions, it is possible to measure the modulus of elasticity values. Fig. 11b presents Young's modulus results obtained in the ultra-micro hardness tester for each composition of the sintered samples. The samples exhibited a variation trend for

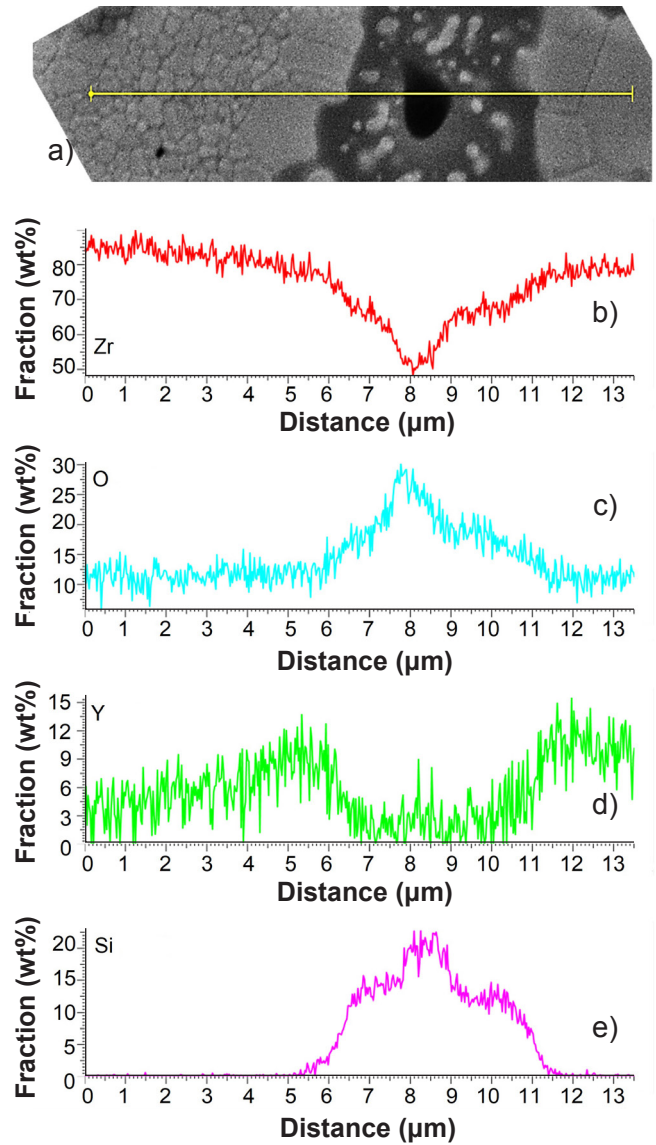


Figure 10: SEM micrograph (a) and EDS line scan profiles for Zr (b), O (c), Y (d), and Si (e) of the line indicated in (a) for the sample with 5 wt% SiO₂ sintered at 1500 °C-2 h.

all groups of samples, where they presented higher values at the lowest loads (250 mN) and decreased as the loads increased, with their lowest values recorded at the highest load (1960 mN). The monolithic 3Y-TZP samples sintered at 1500 °C-2 h showed a modulus of elasticity of around 174 GPa with values varying between 243.6 and 118.6 GPa for the different applied indentation loads. In the sample group ZrO₂-5 wt% SiO₂, an average value of E=170 GPa was obtained with variations between 221 and 138 GPa, indicating a profile similar to the monolithic ceramics. On the other hand, with the increase of SiO₂ in the mixture (ZrO₂-10 wt% SiO₂) there was also an increase in the modulus of elasticity, with an average value of 223 GPa and variations between 280 and 188.5 GPa for indentation loads between 250 and 1960 mN. The results indicate that Young's modulus is a property sensitive to the applied indentation load, due to the tendency to reduce its value with increasing applied load.

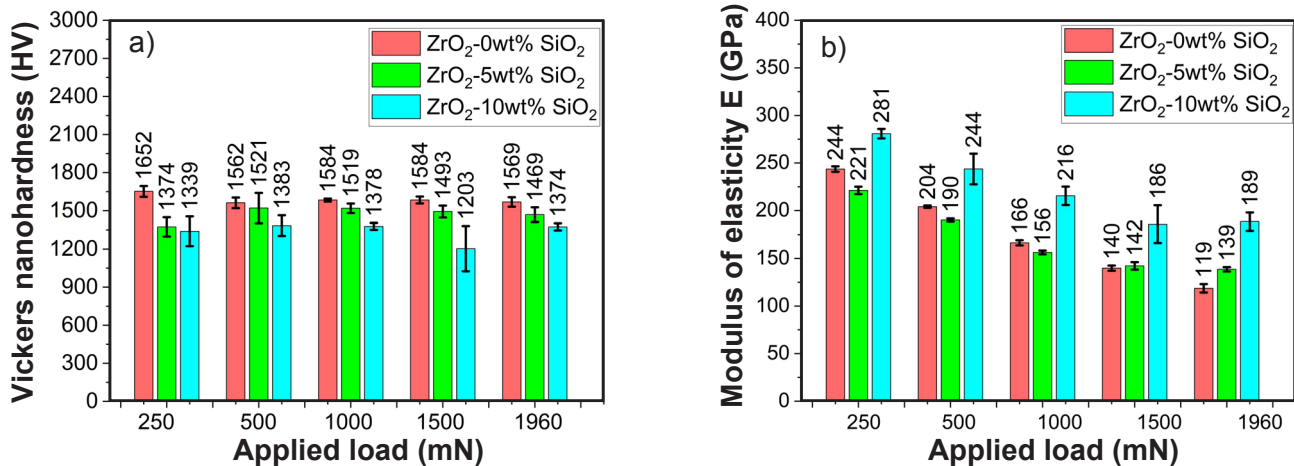


Figure 11: Vickers nanohardness, HV (a), and modulus of elasticity, E (b), by nanoindentation at different indentation loads of samples sintered at 1500 °C-2 h.

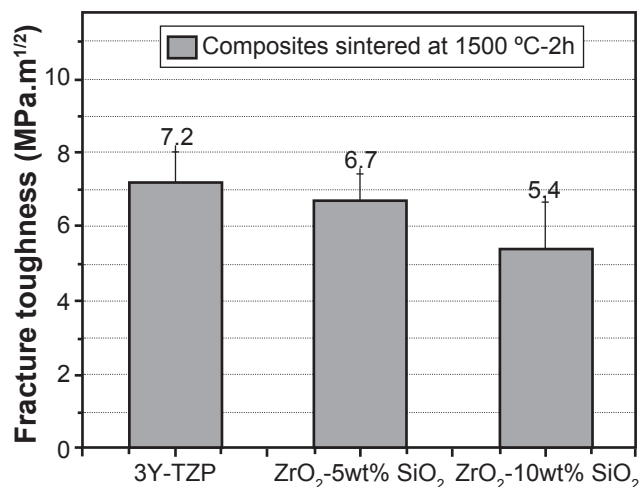


Figure 12: Fracture toughness obtained by the Vickers indentation method for samples sintered at 1500 °C-2 h.

Fracture toughness results obtained by the traditional Vickers indentation technique are presented in Fig. 12. The results indicated that the monolithic ceramics had a mean value of 7.2 ± 0.8 MPa.m^{1/2}, compatible with results observed in the literature that used this characterization technique [42-44]. The addition of silica in the zirconia matrix led to an expected reduction in toughness values, with average values of 6.7 ± 0.5 and 5.4 ± 1.0 MPa.m^{1/2} for the ZrO₂-5 wt% SiO₂ and ZrO₂-10 wt% SiO₂ compositions, respectively. The results reflected a direct downward trend with the structural and microstructural alterations observed in this work. With an increase in the amount of cubic zirconia and ZrSiO₄ and consequent reduction in the toughening tetragonal-ZrO₂ grains in the composition of ceramics, the result, as expected, was a decrease in fracture toughness. Furthermore, the SiO₂ phase created fragile regions that must be controlled so that they do not become potential weakening for future dental applications, but possibly allow increased adhesion with the resin cement. Therefore, adjustments in homogenization must be made, associating mechanical resistance with improvements in adhesion.

CONCLUSIONS

Zirconia mixtures with 5% and 10% by weight of SiO₂ resulted in sintered ceramics composed of complex microstructures, where there were heterogeneous silica regions surrounded by ZrSiO₄, which in turn interfaced with large grains characteristic of the cubic zirconia phase, immersed in a matrix composed mainly of small grains typical of the tetragonal-ZrO₂ phase. This complex microstructural configuration led to a slight reduction in hardness and fracture toughness values. Therefore, improvement in the processing and homogenization of powder mixtures should be sought. On the other hand, the presence of ZrSiO₄ and SiO₂ in the microstructure, phases that have greater chemical affinities with resin cement than zirconia, can improve the adhesion of this composite to dental materials, requiring future confirmation.

ACKNOWLEDGMENTS

The authors would like to thank LABNANO/CBPF for technical support during the electron microscopy analysis. Dr. Claudinei dos Santos recognized FAPERJ (grant E26-202.997/2017) and CNPq (grant 311119/2017-4).

REFERENCES

- [1] I. Denry, J.R. Kelly, *Dent. Mater.* **24**, 3 (2008) 299.
- [2] T. Vagkopoulou, S.O. Koutayas, P. Koidis, J.R. Strub, *Eur. J. Esthet. Dent.* **4**, 2 (2009) 130.
- [3] C. Santos, C.N. Elias, *Rev. Bras. Implantod.* **13**, 3 (2007) 13.
- [4] J. Chevalier, L. Gremillard, A.V. Virkar, D.R. Clarke, *J. Am. Ceram. Soc.* **92**, 9 (2009) 1901.
- [5] J. Luo, R. Stevens, *J. Am. Ceram. Soc.* **82**, 7 (1999) 1922.
- [6] C. Piconi, G. Maccauro, *Biomaterials* **20**, 1 (1999) 1.
- [7] H. Wang, M.N. Aboushelib, A.J. Feilzer, *Dent. Mater.* **24**, 5 (2008) 633.
- [8] M.N. Aboushelib, C.J. Kleverlaan, A.J. Feilzer, *Dent.*

- Mater. **22**, 9 (2006) 857.
- [9] T. Kosmač, C. Oblak, P. Jevnikar, N. Funduk, L. Marion, Dent. Mater. **15**, 6 (1999) 426.
- [10] A.J. Raigrodski, J. Prosthet. Dent. **92**, 6 (2004) 557.
- [11] J.W. Kim, N.S. Covell, P.C. Guess, E.D. Rekow, Y. Zhang, J. Dent. Res. **89**, 1 (2010) 91.
- [12] R. Andreiuolo, S.A. Gonçalves, K.R.H.C. Dias, Rev. Bras. Odont. **68**, 1 (2011) 49.
- [13] C. Santos, C.H. Habibe, A.F. Habibe, R.O. Magnago, Mater. Sci. Forum **881** (2017) 181.
- [14] A.L.N. Oliveira, C.N. Elias, H.E.S. Santos, C. Santos, R.S. Biasi, Int. J. Biomater. **2022** (2022) 11.
- [15] S. Lawson, J. Eur. Ceram. Soc. **15**, 6 (1995) 485.
- [16] J.R. Kelly, I. Denry, Dent. Mater. **24**, 3 (2008) 289.
- [17] L.R. Namoratto, R.S. Ferreira, R.A.V. Lacerda, H.R.S. Filho, F.P. Ritto, Rev. Bras. Odont. **70**, 2 (2014) 142.
- [18] P.F.G. Oliveira, T.B. Rabello, Rev. Bras. Odont. **74**, 1 (2017) 36.
- [19] J.Y. Kim, J.S. Hardy, K.S. Weil, J. Mater. Res. **20**, 3 (2005) 636.
- [20] R.C. de Oyagüe, F. Monticelli, M. Toledano, E. Osorio, M. Ferrari, R. Osorio, Dent. Mater. **25**, 2 (2009) 172.
- [21] A.P. Manso, N.R. Silva, E.A. Bonfante, T.A. Pegoraro, R.A. Dias, R.M. Carvalho, Dent. Clin. **55**, 2 (2011) 311.
- [22] S.S. Atsu, M.A. Kilicarslan, H.C. Kucukesmen, P.S. Aka, J. Prosthet. Dent. **95**, 6 (2006) 430.
- [23] R.C. Oyagüe, F. Monticelli, M. Toledano, E. Osorio, M. Ferrari, R. Osorio, Dent. Mater. **25**, 3 (2009) 392.
- [24] G.M. Reitz, O.R.K. Montedo, E. Comini, K.B. Mundstock, D. Hotza, A.P. Novaes de Oliveira, Cerâm. Ind. **13**, 6 (2008) 1.
- [25] Y. Shi, X. Huang, D. Yan, Ceram. Int. **23**, 5 (1997) 457.
- [26] C.B. Carter, M.G. Norton, *Ceramic materials: science and engineering*, Springer (2007) 345.
- [27] N.M. Rendtorff, G. Suárez, Y. Sakka, E.F. Aglietti, Ceram. Int. **40**, 3 (2014) 4461.
- [28] D.R. Spearing, J.Y. Huang, J. Am. Ceram. Soc. **81**, 7 (1998) 1964.
- [29] T. Ebadzadeh, M. Valefi, J. Alloys Compd. **448**, 1-2 (2008) 246.
- [30] N.M. Rendtorff, S. Grasso, C. Hu, G. Suarez, E.F. Aglietti, Y. Sakka, Ceram. Int. **38**, 3 (2012) 1793.
- [31] G. Yang, J.C. Li, G.C. Wang, S.L. Min, T.C. Chen, M. Yashima, Metall. Mater. Trans. A **37** (2006) 1969.
- [32] C. Santos, I.F. Coutinho, J.E.V. Amarante, M.F.R.P. Alves, M.M. Coutinho, C.R.M. Silva, J. Mech. Behav. Biomed. Mater. **116** (2021) 104372.
- [33] B. Almutairi, M. Binhasan, S. Shabib, A.S. Al-Qahtani, H.I. Tulbah, K.A. Al-Aali, F. Vohra, T. Abduljabbar, Int. J. Adhes. Adhes. **114** (2022) 103069.
- [34] ISO 6872, “Dentistry: ceramic materials”, Geneva (2015).
- [35] A.C.D. Chaklader, A.L. Roberts, J. Am. Ceram. Soc. **44**, 1 (1961) 35.
- [36] I. Yanase, M. Miyagi, H. Kobayashi, J. Eur. Ceram. Soc. **29**, 15 (2009) 3129.
- [37] S. Maj, Phys. Chem. Miner. **15**, 3 (1988) 271.
- [38] L.G. Abreu, M.N. Quintino, M.F.R.P. Alves, C.H. Habibe, A.S. Ramos, C. Santos, J. Mater. Res. Technol. **9**, 5 (2020) 10830.
- [39] Shimadzu, “Dynamic ultra micro hardness testers system for evaluating thin films, surface-treated layers, and microelectronic parts, dynamic ultra micro hardness testers”, C227-E024C (2023) 7.
- [40] ASTM C20-17, “Standard test methods for apparent porosity, water absorption, apparent specific gravity, and bulk density of burned refractory brick and shapes by boiling water”, Am. Soc. Test. Mater. (2017).
- [41] Shimadzu, “Dynamic ultra-micro-hardness tester DUH-211/DUH-211S instruction manual” (2009).
- [42] J.E.V. Amarante, M.V.S. Pereira, G.M. Souza, M.F.R.P. Alves, B.G. Simba, C. Santos, J. Mech. Behav. Biomed. Mater. **109** (2020) 103847.
- [43] F. Kern, A. Kabir, R. Gadow, Ceram. Mater. **69** (2017) 279.
- [44] W. Zhao, C. Peng, M. Lv, M. Bai, P. Rao, Ceram. Int. **41**, 1 (2015) 869.

(Rec. 10/07/2023, Rev. 03/10/2023, Ac. 21/10/2023)

